Electronic Supplementary Information

Flexible Quasi-Solid-State Planar Micro-supercapacitors Based on Cellular Graphene films

[1, 2, 3]Yuanlong Shao*, [2]Jianmin Li [4]Yaogang Li, [2]Hongzhi Wang, [2]Qinghong Zhang [1,]

[5]Richard B. Kaner*

[1]*Department of Chemistry and Biochemistry and California NanoSystems Institute, University of California, Los Angeles (UCLA), Los Angeles, California 90095, USA*

[2]*State Key Laboratory for Modification of Chemical Fibers and Polymer Materials, College of Material Science and Engineering, Donghua University, Shanghai, 201620, China*

[3]*Present address: Cambridge Graphene Center, Department of Engineering, University of Cambridge, Cambridge, CB3 0FA, UK*

[4]*Engineering Research Center of Advanced Glasses Manufacturing Technology, Ministry of Education, Donghua University, Shanghai, 201620, China*

[5]*Department of Materials Science and Engineering, UCLA, Los Angeles, California 90095, USA.*

CORRESPONDING AUTHOR:

* Dr. Yuanlong Shao E-mail: yuanlong.shao@gmail.com

* Dr. Richard B. Kaner E-mail: kaner@chem.ucla.edu

1. Experimental Section

Synthesis of cellular graphene films: 3D porous graphene films were prepared by a freeze-casting assisted filtration assembly method, as reported in our earlier work.[1] Typically, graphene oxide (GO) was suspended in water to give a homogeneous aqueous dispersion with a concentration of 3 mg ml^{-1}. Then 1 ml of GO dispersion was mixed with 7 mg of ascorbic acid. After being vigorously shaken for a few minutes, the mixture was then placed in a 50 °C oven for 30 minutes to obtain partially reduced GO. The partially reduced GO dispersion was assembled into films by vacuum assisted filtration and immersed into a liquid nitrogen bath for 30 minutes. Then the film was placed in a 100 °C oven for 12 hours for further reduction. The obtained reduced GO film were transferred into a Petri dish and washed with deionized water several times to remove any remaining ascorbic acid, followed by freeze-drying for 24 h to form fully dried 3D porous reduced GO films.

Fabrication of sandwich-structured supercapacitors and MSCs: The as-fabricated reduced GO films were cut into 1 cm × 1 cm square pieces and immersed into 1.0 M H_2SO_4 aqueous electrolyte overnight to exchange their interior water with electrolyte. Then two pieces of reduced GO films were separated by a polypropylene separator, assembled into a sandwich architecture and tightly sealed with Kapton tape to create each MSC.

The interdigitated pattern for the MSCs was created using laser lithography with a CO_2 laser platform (Full Spectrum CO_2 hobby laser). The interdigitated patterns for the MSCs were created using laser lithography with a CO_2 laser platform (Full Spectrum CO_2 laser, laser wavelength 10.6 μm). The fully dried 3D porous reduced GO film was glued to the surface of a commercial polyethylene terephthalate (PET) sheet (3M PP2950 transparency films) with a thickness of 108 μm as a flexible substrate for the micro-supercapacitors. PET sheets were first cleaned with water and ethanol three times before spraying on the glue. The glue (Scotch Spray Mount, Repositionable adhesive) was evenly sprayed onto the PET substrate to ensure that the electrode films were firmly fixed onto the flexible substrates. The laser ablation process on the 3D porous reduced GO films was carried out by adjusting the irradiation laser power between 200 mW to

400 mW. The laser-writing process was conducted following the designed pattern and power controlled by a computer program. All of the laser writing experiments were performed in air under ambient conditions with flowing nitrogen. After laser ablation, the remaining parts of the film served as both the active electrodes and the current collectors. Silver ink was painted between the edge of the patterned cellular graphene films and conductive copper tape to decrease the contact resistance. The Kapton tape was used to cover the exposed copper tape to avoid corrosion by the electrolyte, especially when voltage is applied. An aqueous electrolyte of 1.0 M H_2SO_4 was then placed on the surface and allowed to infiltrate overnight before electrochemical characterization. Quasi-solid-state MSCs were fabricated by simply switching a PVA/H_3PO_4 gel electrolyte for the aqueous electrolyte. The PVA/H_3PO_4 gel electrolyte was fabricated according to a previous report.[2]

Characterization: The morphology and microstructure of the prepared films were investigated by means of field emission scanning electron microscopy (FE-SEM, JEOL 6701F). Tensile strength of each film was tested on a tensile testing machine (Q800 DMA (Dynamic Mechanical Analyzer)).

Electrochemical measurements and calculations: All the electrochemical experiments were carried out using a two-electrode system with a Bio-Logic VMP3 potentiostat. Cyclic voltammetry (CV) and galvanostatic charge/discharge (GCD) experiments were carried out with a potential window of 1.0 V for both aqueous and gel electrolytes. The EIS measurements were performed at open circuit potential with a sinusoidal signal over a frequency range from 1 MHz to 10 mHz at an amplitude of 10 mV. The cycle life tests were conducted by GCD measurements.

The areal specific capacitance was calculated from the CV data based on equation [1]:

$$C = \frac{\int i\, dV}{S\, V\, v} \text{ (mF cm}^{-2}\text{)} \qquad [1]$$

where i is the discharge current in the negative CV curve, v is the scan rate, S is the total area of the planar substrate (including the interval spaces between the interdigited electrodes, 1.46 cm^{-2}), and V represents the potential window.

The areal specific energy density and power density were calculated using equations [2]

and [3], respectively:

$$E = \frac{C\,\Delta V^2}{7200} \quad (\text{mWh cm}^{-2}) \qquad [2]$$

$$P = \frac{E\ 3600}{\Delta t} \quad (\text{mW cm}^{-2}) \qquad [3]$$

where the voltage ΔV is the voltage drop upon discharge in the negative CV curve, Δt is the discharge time, E is the areal energy density (mWh cm^{-2}), and P is the areal power density (mW cm^{-2}).

The measured Nyquist plots were well fit based on using software ZView® with the following equation [4]:

$$\mathrm{Z} = R_s + \frac{1}{j\omega C_{dl} + \frac{1}{R_{ct} + W_0}} + \frac{1}{j\omega C_l} \qquad [4]$$

where R_s is the cell internal resistance, C_{dl} is the double layer capacitance, R_{ct} is the charge transfer resistance, W_o is the Warburg element, and C_l is the low frequency mass capacitance. As illustrated in Supplementary Figure S6a, these resistor and capacitor elements in the equivalent circuit are related to specific parts in the Nyquist plot. At high frequency, the point of intersection on the real axis represents the internal resistance R_s, which includes the intrinsic electronic resistance of the electrode material, the ohmic resistance of the electrolyte, and the interfacial resistance between the electrode and the current collector. The semicircle in the high frequency region provides the behavior of the interfacial charge transfer resistance R_{ct} and the double layer capacitance C_{dl}. After the semicircle, the Nyquist plot exhibits a straight long tail almost perpendicular to the x-axis and stretching to the low frequency region. This almost ideal vertical line represents the mass capacitance C_l. The transmission line with an angle of nearly 45 degrees to the x-axis from the high frequency to the mid-frequency represents the Warburg element W_o, which is expressed as equation [5]:

$$W_o = \frac{A}{(j\omega)^n} \qquad [5]$$

where A is the Warburg coefficient, ω is the angular frequency, and n is an exponent. All the values fit using these elements are summarized in Supplementary Table S1.

This fitting and analysis process have been described in our previous research.[1]

2. Supplementary Tables

Supplementary Table S1. Equivalent Circuit Parameters[a] for Different Supercapacitor Designs.

Fitting Parameters	$R_s(\Omega)$	$R_{ct}(\Omega)$	C_{dl} ($\mu F/cm^2$)	$A(\Omega . S^{-n})$	n
Sandwich structured supercapacitor	19.78	7.25	2.49	50.37	0.47
MSC	5.36	2.31	10.32	12.16	0.47
Quasi-solid state MSC	16.63	37.69	4.05	141.4	0.30

[a]Obtained from the fitting results for components of the equivalent circuit fit with the impedance spectra.

Supplementary Table S2. Comparison of Performances for Graphene Based MSCs.

Device	Systems	Areal capacitance (mF cm^{-2})	Areal Energy density (μWh cm^{-2})	Areal Power density (mW cm^{-2})	Thickness (μm)	Flexibility (retention ratio)	constant time (ms)	Ref.
Aqueous electrolyte based MSC	***Cellular Graphene (1M H_2SO_4)***	***2.47***	***0.34***	***5.3***	***19.4***	***na***	***82.9***	***This work***
	Laser reduced graphene	0.51	0.014	0.009	20	97% (2,000 cycles under bent or twisted state)	na	[3]
	Graphene quantum dots (EMIMBF_4/AN)	0.468	0.474	0.057	0.312	na	0.0538	[4]
	Graphene/CNT carpets (1M Na_2SO_4)	2.16	0.32	23	20	na	0.402	[5]
	Onion-like carbon (1M Et_4NBF_4)	0.9	0.012	1.96	7	na	26	[6]
	Reduced GO/CNT (3M KCl)	2.8	0.408	46.2	6	na	3.4	[7]
	Vertically Aligned Graphene (EMIMBF_4)	7.3	0.98	42.8	3.5	na	18	[8]
	Graphene/Phosphorene (BMIMPF_6)	9.8	2.32	0.3	2	89.5% of maximum capacitance (2,000 cycles, constant bending state	na	[9]
	Vertically oriented Graphene (Phosphonium ionic liquid)	2.0	na	na	na	na	na	[10]
Quasi-	***Cellular Graphene***	***1.7***	***0.22***	***0.37***	***19.4***	***89.4% (1,000 bending***	***1,670***	***This***

solid-state	***(PVA/H_3PO_4)***					***cycles from 0 to 120°)***		***work***
MSC	Graphene (PVA/H_2SO_4)	0.081	0.037	0.74	0.015	na	0.28	[11]
	Exfoliated Graphene/PH1000 (PVA/H_2SO_4)	5.4	na	na	1.5	98.5% (1,000 cycles under bending radius of 5 mm)	na	[12]
	Vertically Aligned Graphene (PVA/H_2SO_4)	3.4	0.56	10.5	3.5	na	9	[8]
	Arbitrary-shaped graphene	19.7	1.45	1.15	5	No change on bending curvature radii from 42 to 2 mm	na	[13]
	Photochemically Reduced Graphene (PVA/H_2SO_4)	1.5	0.0095	0.52	0.063	93.7% (from 0 to 180°) Nearly 100% (4,000 cycles under 180° bending)	25.9	[14]
	S-doped graphene film (PVA/H_2SO_4)	0.55	0.0031	1.19	0.010	na	0.26	[15]
	Laser-processed graphene (PVA/LiCl)	3.9	1.76	0.54	18	negligible changes under bending states from 0 to 180°	na	[16]
	MoS_2@rGO-CNT (PVA/H_2SO_4)	13.7	1.9	na	3.4	na	na	[17]
	3D porous Graphene (PVA/H_2SO_4)	2.4	0.38	0.86	70	85% (5,000 cycles at a 90° bending angle)	na	[18]
	Laser induced graphene/MnO_2 (PVA/LiCl)	934	32.4	2.33	101	90% (10,000 bending cycles with 90°)	na	[19]

3. Supplementary Figures

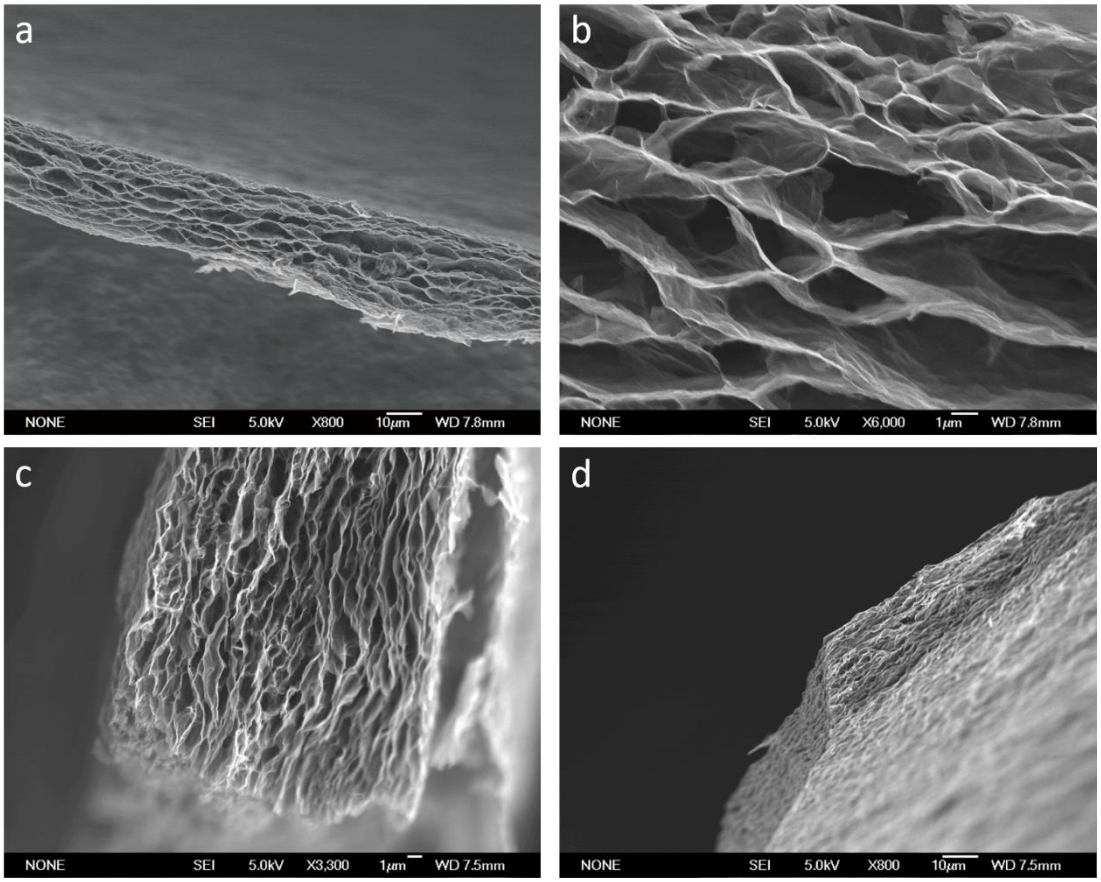

Supplementary Figure S1. (a) Cross-section SEM images of a cellular graphene film. (b) Partially enlarged views of (a) under higher magnification. (c, d) Cross-section SEM images of the edges of a cellular graphene film.

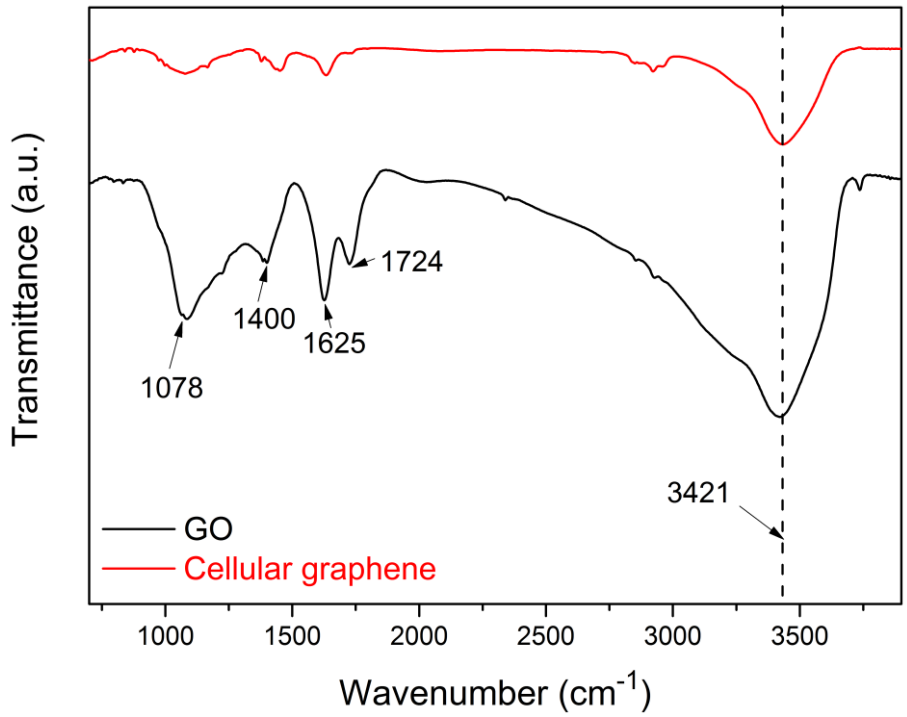

Supplementary Figure S2. Comparison of FT-IR spectra for GO and cellular graphene film.

To further confirm the reduction of the cellular graphene film, FT-IR analyses of GO and cellular graphene were performed as shown in Figure S2. The most significant absorption peaks around 3500 cm^{-1} can be assigned to O-H stretching vibrations due to the hydroxyl groups. The dampening and subsequent shift of the peak shows the involvement of the O-H group in the reduction. Absorption due to the C=O group (1725 cm^{-1}) decreased in intensity and the absorptions at 1635 cm^{-1} (O-H group) are absent, suggesting that the carboxyl groups on the surface of have been reduced or modified. In addition, the decrease in the intensity of the deformation peak for the O-H group at 1400 cm^{-1} and the C-O (alkoxy) stretching vibration peak at 1078 cm^{-1} also indicate the reduction of the cellular graphene film after thermal treatment.

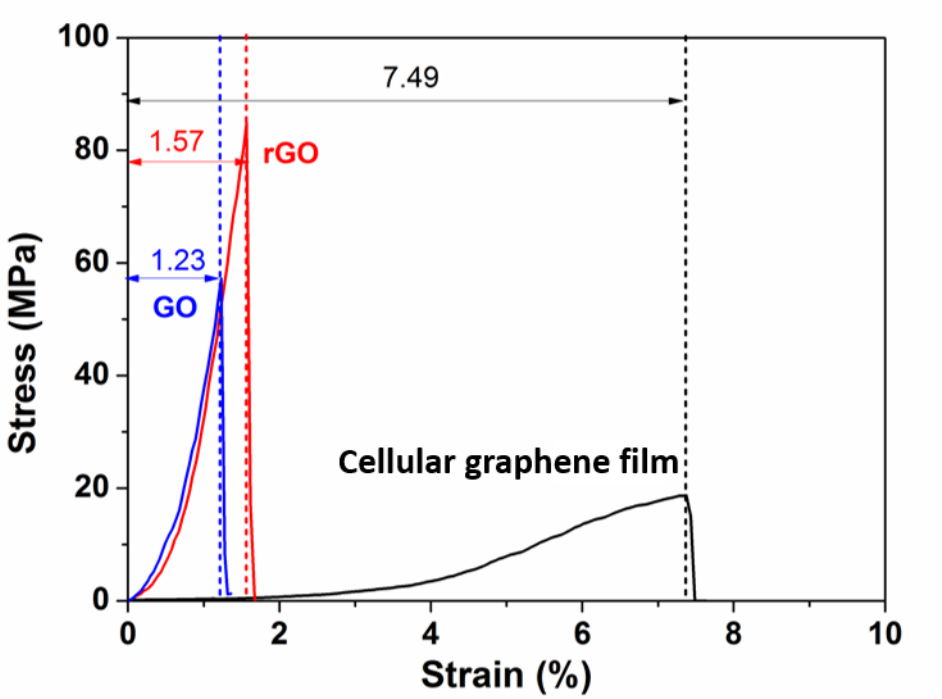

Supplementary Figure S3. Stress-strain curves for a cellular graphene film, a GO film and a reduced GO film.

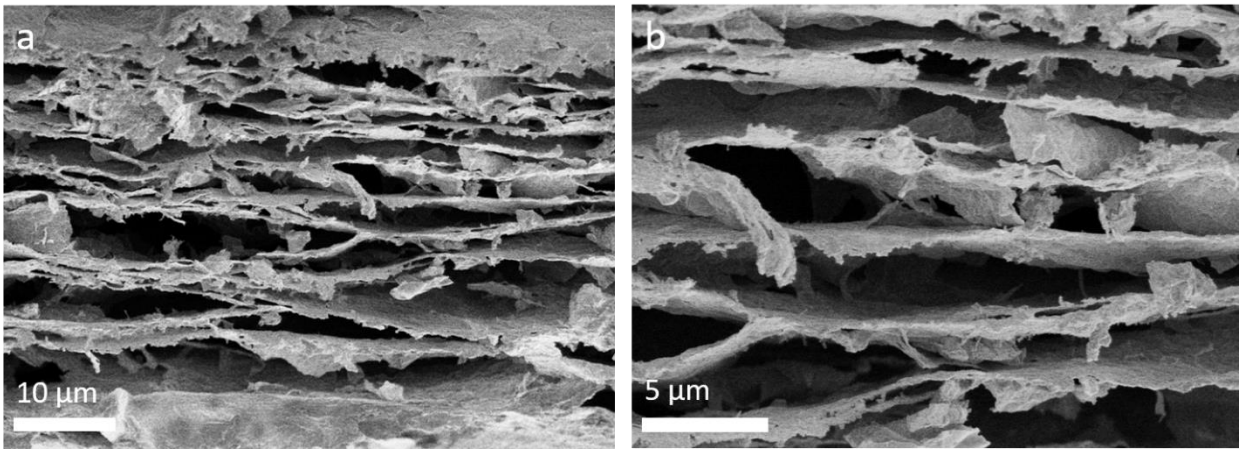

Supplementary Figure S4. (a, b) Cross-sectional SEM images of cellular graphene after laser ablation.

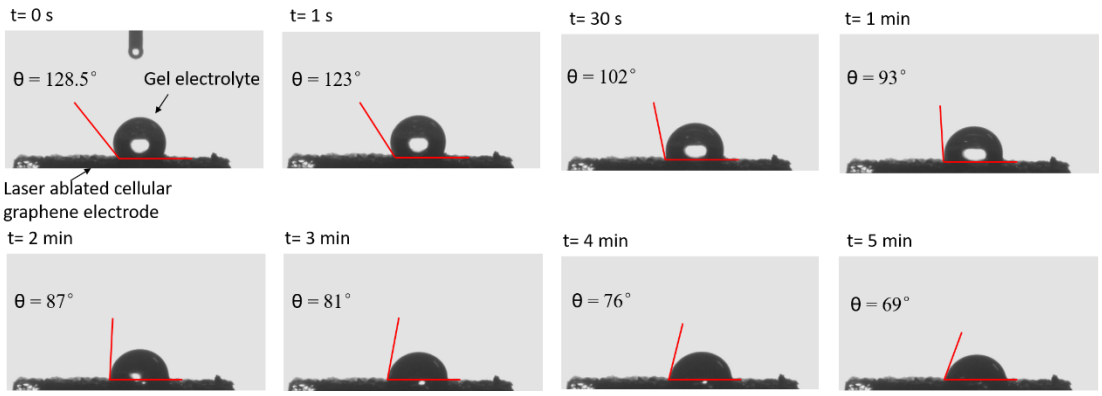

Supplementary Figure S5. The optical images of the wetting angles for the gel electrolyte on the laser ablated cellular graphene electrode with different times.

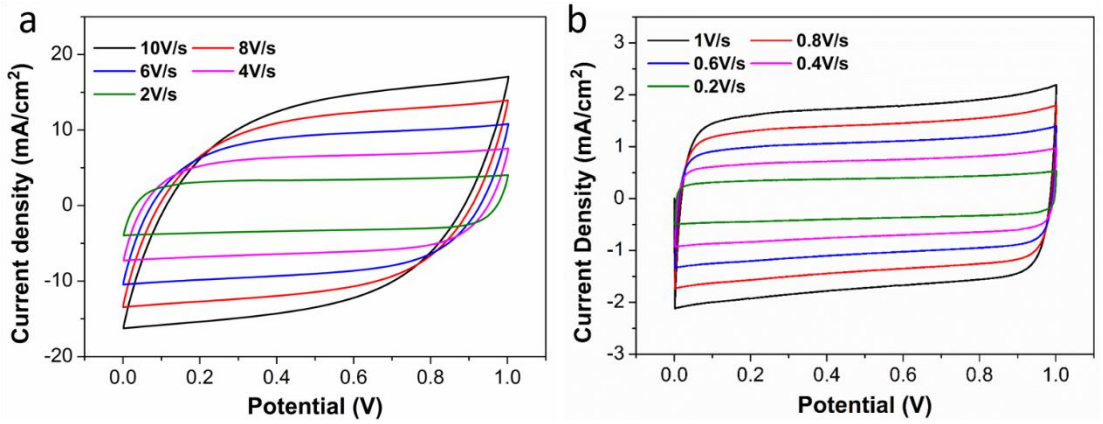

Supplementary Figure S6. CV curves of a cellular graphene based MSC with scan rates ranging from 0.2 to 10 V s^{-1}.

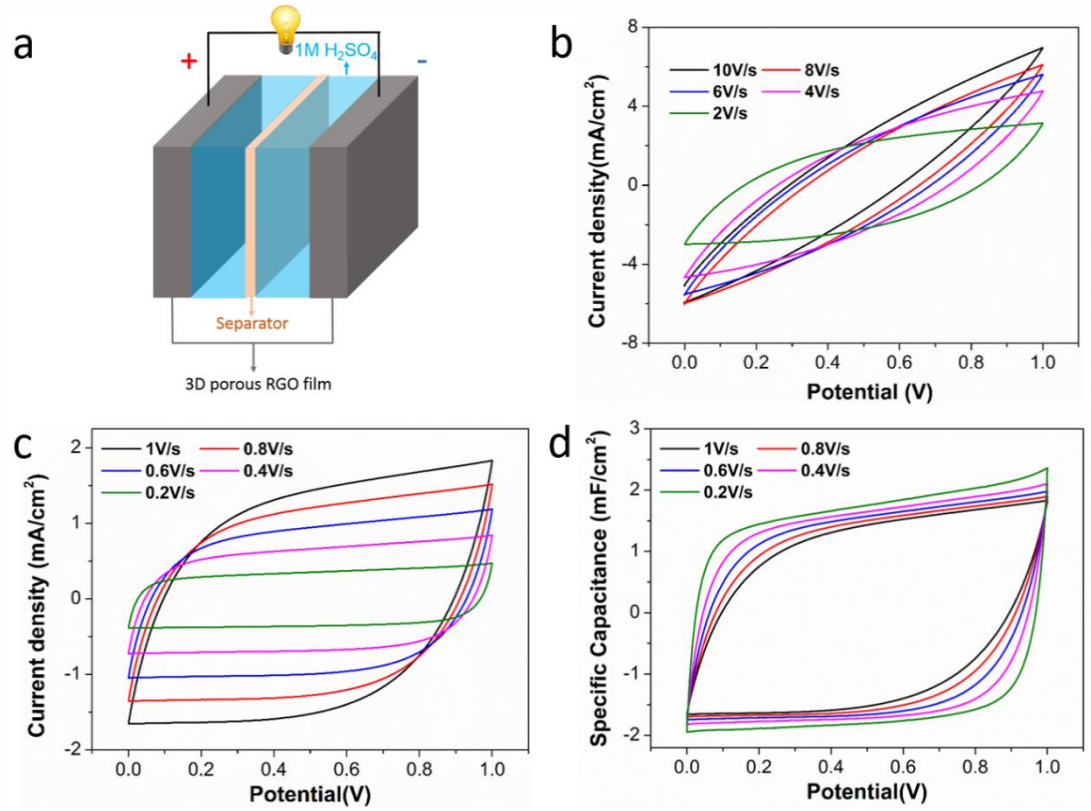

Supplementary Figure S7. (a) Schematic illustration of a sandwich structured supercapacitor, (b-d) CV curves of a sandwich structured supercapacitor with scan rates ranging from 0.2 to 10 V s^{-1}.

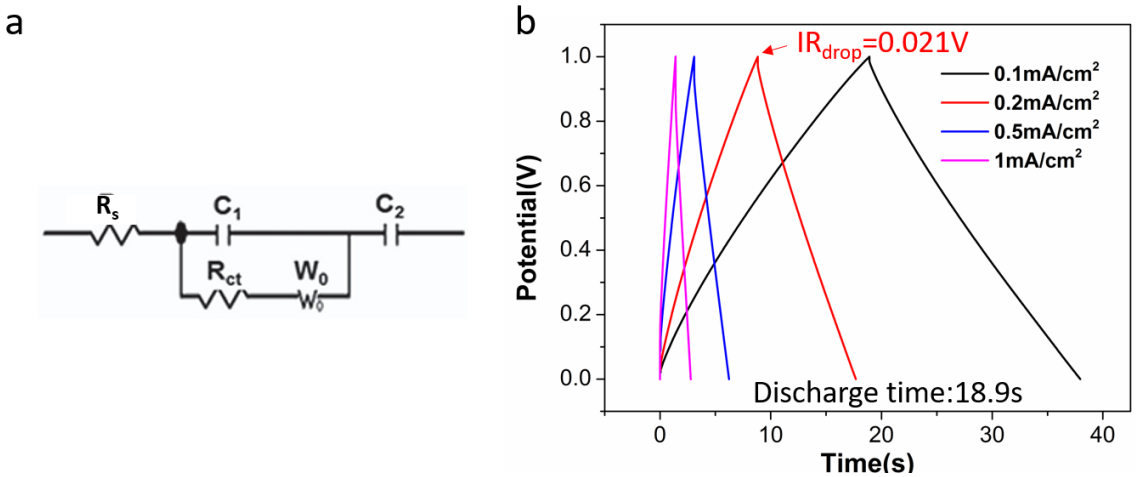

Supplementary Figure S8. (a) A Randles equivalent circuit for Nyquist plot fitting. (b) Galvanostatic charge/discharge profiles of a sandwich structured supercapacitor with various current densities ranging from 0.1 to 1 mA cm^{-2}.

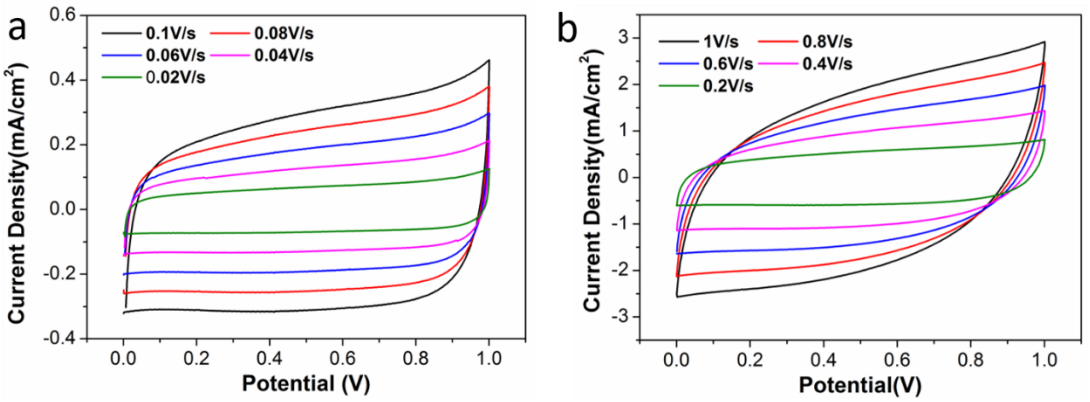

Supplementary Figure S9. CV curves of a quasi-solid-state MSC with scan rates ranging from 0.02 to 1 V s^{-1}.

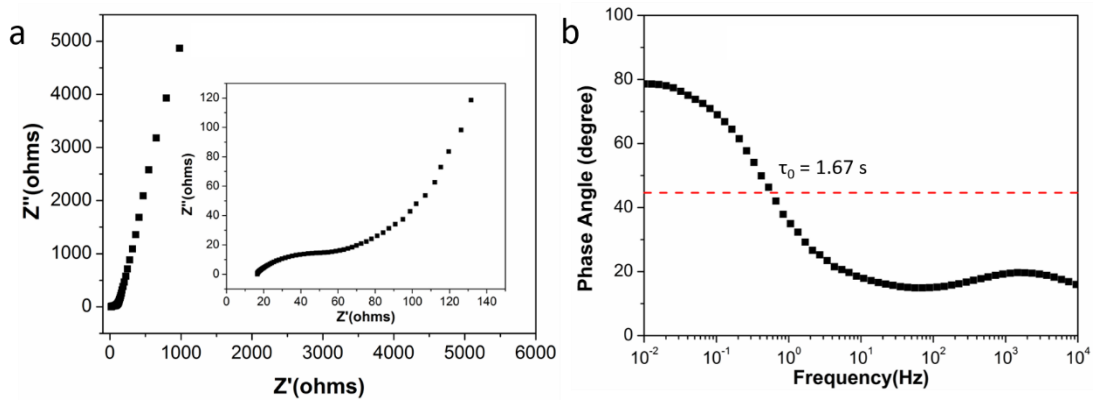

Supplementary Figure S10. A Nyquist plot and a Bode plot of a quasi-solid-state MSC. The inset in (a) shows the magnified high-frequency region.

References:

1. Y. Shao, M. F. El-Kady, C.-W. Lin, G. Zhu, K. L. Marsh, J. Y. Hwang, Q. Zhang, Y. Li, H. Wang and R. B. Kaner, *Adv. Mater.*, 2016, **28**, 6719-6726.
2. Y. Shao, H. Wang, Q. Zhang and Y. Li, *NPG Asia Mater*, 2014, **6**, e119.
3. W. Gao, N. Singh, L. Song, Z. Liu, A. L. M. Reddy, L. Ci, R. Vajtai, Q. Zhang, B. Wei and P. M. Ajayan, *Nat. Nanotechnol.*, 2011, **6**, 496-500.
4. W.-W. Liu, Y.-Q. Feng, X.-B. Yan, J.-T. Chen and Q.-J. Xue, *Adv. Funct. Mater.*, 2013, **23**, 4111-4122.
5. J. Lin, C. Zhang, Z. Yan, Y. Zhu, Z. Peng, R. H. Hauge, D. Natelson and J. M. Tour, *Nano Lett.*, 2012, **13**, 72-78.
6. D. Pech, M. Brunet, H. Durou, P. Huang, V. Mochalin, Y. Gogotsi, P.-L. Taberna and P. Simon, *Nat. Nanotechnol.*, 2010, **5**, 651-654.
7. M. Beidaghi and C. Wang, *Adv. Funct. Mater.*, 2012, **22**, 4501-4510.
8. S. Zheng, Z. Li, Z.-S. Wu, Y. Dong, F. Zhou, S. Wang, Q. Fu, C. Sun, L. Guo and X. Bao, *ACS Nano*, 2017, **11**, 4009-4016.
9. H. Xiao, Z.-S. Wu, L. Chen, F. Zhou, S. Zheng, W. Ren, H.-M. Cheng and X. Bao, *ACS Nano*, 2017, **11**, 7284-7292.
10. J. R. Miller and R. A. Outlaw, *J. Electrochem. Soc.*, 2015, **162**, A5077-A5082.
11. Z. S. Wu, K. Parvez, X. Feng and K. Müllen, *Nat. Commun.*, 2013, **4**, 2487.
12. Z. Liu, Z.-S. Wu, S. Yang, R. Dong, X. Feng and K. Müllen, *Adv. Mater.*, 2016, **28**, 2217-2222.
13. S. Zheng, X. Tang, Z.-S. Wu, Y.-Z. Tan, S. Wang, C. Sun, H.-M. Cheng and X. Bao, *ACS Nano*, 2017, **11**, 2171-2179.
14. S. Wang, Z.-S. Wu, S. Zheng, F. Zhou, C. Sun, H.-M. Cheng and X. Bao, *ACS Nano*, 2017, **11**, 4283-4291.
15. Z.-S. Wu, Y.-Z. Tan, S. Zheng, S. Wang, K. Parvez, J. Qin, X. Shi, C. Sun, X. Bao, X. Feng and K. Müllen, *J. Am. Chem. Soc.*, 2017, **139**, 4506-4512.
16. B. Xie, Y. Wang, W. Lai, W. Lin, Z. Lin, Z. Zhang, P. Zou, Y. Xu, S. Zhou, C. Yang, F. Kang and C.-P. Wong, *Nano Energy*, 2016, **26**, 276-285.
17. W. Yang, L. He, X. Tian, M. Yan, H. Yuan, X. Liao, J. Meng, Z. Hao and L. Mai, *Small*, 2017, **13**, 1700639.
18. L. Zhang, D. DeArmond, N. T. Alvarez, R. Malik, N. Oslin, C. McConnell, P. K. Adusei, Y.-Y. Hsieh and V. Shanov, *Small*, 2017, **13**, 1603114.
19. L. Li, J. Zhang, Z. Peng, Y. Li, C. Gao, Y. Ji, R. Ye, N. D. Kim, Q. Zhong, Y. Yang, H. Fei, G. Ruan and J. M. Tour, *Adv. Mater.*, 2016, **28**, 838-845.